A Superconducting Spiral Bandpass Filter designed by a ~~pseudo~~Pseudo-Fourier Technique

Frederick Huang[1*], Pietro Bolli[2], Luca Cresci[2], Sergio Mariotti[3], Dario Panella[2], Jose A. Lopez-Perez[4], and Pablo Garcia[4]

[1] Department of Electronic, Electrical and Systems Engineering, University of Birmingham, Edgbaston, Birmingham, B15 2TT, United Kingdom
[2] Arcetri Astrophysical Observatory, National Institute for Astrophysics, Largo E. Fermi 5, Florence, Italy
[3] Institute of Radio Astronomy, National Institute for Astrophysics, via P. Gobetti 101, Bologna, Italy
[4] ~~Jefe de Servicio del Centro Astronomico~~Observatorio de Yebes, Dir. Gral. Instituto Geografico Nacional, Apartado 148, E-19080 Guadalajara, Spain.
*f.huang@bham.ac.uk

Abstract: An iterative technique to adjust ripple in a Bandpass filter has been developed by curve fitting numerical data. It gives an approximate relation of ripple against filter coupling coefficients and resonator resonant frequencies instead of finding a Jacobian Matrix for each individual filter, in exchange for making more iterations. Numerical examples show reasonable convergence for Chebyshev filters up to 16th order, coupled quadruplets, coupled triplets, and folded cross-coupled filters. A band-pass filter for a radio telescope in Yebes, Spain is designed and measured, a 10th order superconducting spiral filter with 7 percent bandwidth, 2295 MHz centre frequency, less than 0.1dB ripple and overall substrate size 30 mm x 8 mm.. The 11 iterative simulations totalled 8.5 hours of CPU time.

1. Introduction

Microwave filter design is well established [1], [2], but the filters often need a final iterative fine-tuning stage, in which ripple errors in simulation results or measured data are used to find corrections in the resonator centre frequencies and coupling coefficients. This is particularly important in planar structures such as microstrips where the resonators are not isolated in separate compartments, so there is coupling between non-adjacent resonators, not considered in the original design.

One method in its simplest form involves finding a Jacobian matrix which gives the gradients of resonator resonant frequencies and coupling coefficients with respect to ripple depths; the necessary adjustments for each iteration follow directly. Similar optimisation algorithms are [3], [4], [5] [6] and [7]. In another approach [8], [9] particularly suitable for tuning a filter after fabrication, all resonators are deliberately detuned, and then adjusted one by one to have the correct response. In [9], when tuning any one resonator, all those already adjusted have a known response, while those not yet tuned are either purely inductive or capacitive and therefore at least have a known phase and group delay response. Finally, time domain tuning, where resonators can also be tuned one by one, independent of each other, has been introduced [10].

In this paper, approximate Jacobian matrix coefficients are introduced as a standard set of equations, greatly reducing the number of simulations, even if more iterations are required. They apply to symmetrical layouts of resonators and coupling coefficients, but the frequency responses need not be symmetrical. They are found by observation of numerical data, which is similar to curve-fitting, so a derivation is not available, but a speculative explanation is suggested. Numerical results based on scattering matrix calculations [1] on Chebyshev filters are given for filter orders between 3rd and 20th order. The equations are also shown to be workable for cross-coupled filters, at a reduced rate of convergence. However, there is no provision yet for adjusting the cross-coupling coefficients, which may have to be determined by trial and error.

Powerful software such as [11] and [12] can be costly; with the very simple equations here, the adjustments can with patience be estimated for filters up to 6th order using a pocket calculator, although an e.m. simulator would still be required to verify the results. Preferably written as a page of software, they should be suitable for designing moderate numbers of filters up to 16th order.

The equations are also demonstrated for a 10th order superconducting spiral bandpass filter for the Yebes radio telescope in Spain. Radio telescopes require cryogenic front-ends to reduce receiver noise, so the superconducting filters do not introduce new cooling needs. At 0.01 – 10 GHz, they are very compact without being significantly lossy. The spiral resonators have large empty spaces at their centres which give a wide stop band [13]. This also reduces non-adjacent coupling, since the distances between non-adjacent resonators can be large compared with adjacent resonators; nevertheless it is significant and influences the design. Apart from the adjacent coupling, there are two capacitive bridges, making two coupled quadruplets (CQ) [14], [15], [16]. Other capacitive bridges mitigate non-adjacent coupling. Two further resonators provide external coupling.

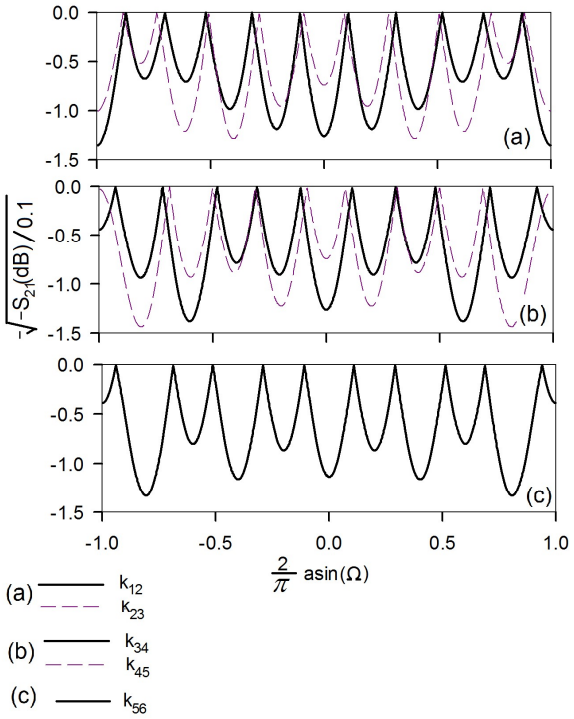

Fig. 1. Pass band ripple of a 10th order Chebyshev filter, originally 0.1 dB ripple but with two coupling coefficients k_{12}, and $k_{10,9}$; or k_{23},and k_{98}; ... 2% too large.

2. The ripple-reduction iterative algorithm

The coupling coefficients $k_{m,m+1}$ (m=1,… N-1) of a 10th order Chebyshev bandpass filter with 0.1dB ripple, zero centre frequency and bandwidth of 2 normalised units is given in table 1, together with the external coupling coefficient k_e, more commonly written as $1/Q_e$, the reciprocal of external quality factor, calculated from data given in [17]. Using coupling matrices [1], the ripple is recalculated 5 times; in each case one of values of $k_{m,m+1}$ and the symmetrically placed $k_{10-m,11-m}$, are in error by a factor of 1.02. The results are shown in Fig. 1. For clarity, the normalised frequency Ω is warped by the inverse sine function, giving the ripples nearly equal width, and depths R_n dB (n=1…N-1, from left to right on the frequency axis), taken to be positive even though they are measured downwards from 0 dB. (For an actual filter, $\Omega=2(f-f_0)/B$, where f_0 is the centre frequency and B the bandwidth.) The envelope enclosing the dips has an approximate cosine variation, with progressively more cycles as the error occurs nearer the centre of the filter. However, ripple resulting from an error in k_e does not follow this pattern in that it does not give a constant ripple error, (i.e. a cosine of constant zero angle); it is considered separately. A similar set of graphs for errors of resonator centre frequencies of 0.02 (normalised units) gives an approximate sinusoidal variation. This suggests a Fourier relationship, with the ripple envelope forming one domain and the filter coupling coefficients and resonance frequencies the other. One significant difference is that coupling errors near the centre of the filter cause the ~~cosines~~envelopes with the fastest variations. Conversely, a sinusoidal variation in the coupling coefficients and resonant frequencies is expected to give an error in one particular ripple. The values of constants can be found from fitting numerical data.

Table I: Normalised coupling coefficients for a 10th order bandpass filter with 0.1 dB ripple

Additional coefficients are determined from symmetry

$1/Q_e$ or k_e	0.8334	k_{34}	0.5355
k_{12}	0.7586	k_{45}	0.5256
k_{23}	0.5675	k_{56}	0.5232

An N^{th} order simulated design (or possibly a measured one) is first deliberately detuned by reducing k_e and k_{12} until all N-1 ripples are visible. Some of the ripples can consequently become large, especially for high order filters. A ripple adjustment function is

$$A_n = (\sqrt{R_0} - \sqrt{R_n})\frac{\alpha}{2N} \qquad (1)$$

where R_0 dB is the target final ripple (and not the initial value as suggested by subscript 0), written here as a constant, but it can have a different value for each ripple. The value α is a constant, usually 1 or less, to improve convergence. For a symmetrical filter, only the resonators on the left side have to be considered; they are labelled from left to right,

$$m = 1 \ldots \frac{N+1}{2} \qquad (2)$$

$$m = 1 \ldots \frac{N}{2} \qquad (3)$$

for N odd and N even respectively; the corrections to the resonance frequencies are

$$\Delta f_m = \frac{-(F_2+F_1)}{2} + \sum_{n=1}^{N-1} A_n \cos\left[\frac{2\pi}{N}\left(m-\frac{1}{2}\right)n\right] \qquad (4)$$

where F_1 is the lower band edge (whose target value is -1) and F_2 the upper band edge (with target 1). The first term is an obvious correction for the centre frequency while the second corrects the ripple. The cosine (instead of sine) function arises from defining n as above, instead of symmetrically as -(*N-1*)/2 … (*N-1*)/2 which may involve half-integer values.

The coupling coefficients are each corrected by two ratios, the first of which are

~~r_e~~ $r_e = \frac{2}{F_2-F_1}$ (5)

$$r_{m,m+1} = \frac{2}{F_2-F_1} - \sum_{n=1}^{N-1} A_n \cos\left[\frac{2\pi}{N}mn\right] \qquad (6)$$

where

$$m = 1 \ldots \frac{N-1}{2} \qquad (7)$$

$$m = 1 \ldots \frac{N}{2} \qquad (8)$$

for N odd and even respectively. The first term scales all coefficients to correct ~~for~~ a bandwidth error.

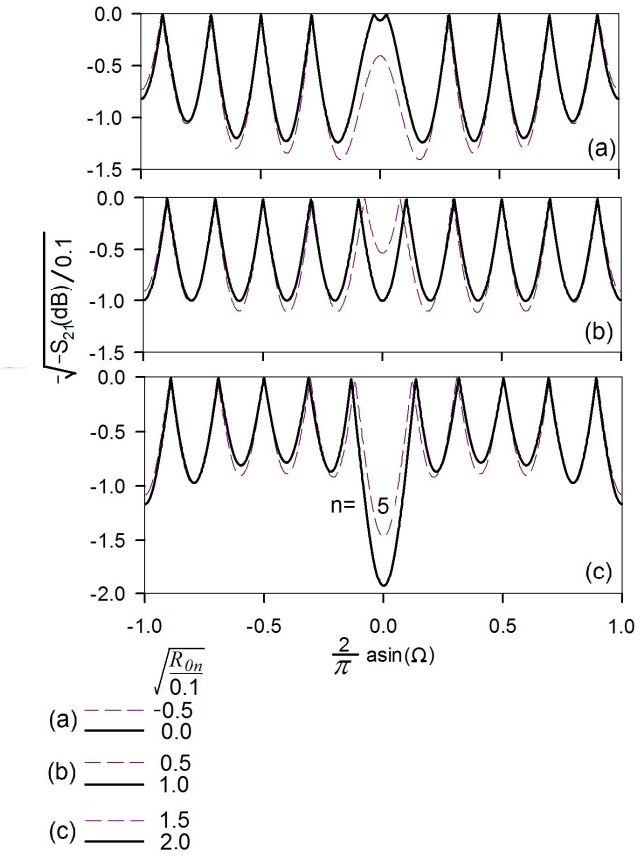

Fig. 2. Result of one iteration on an already optimum filter with all ripple R_n=0.1 dB, resetting the target ripple R_0 for n=5 to a new value.

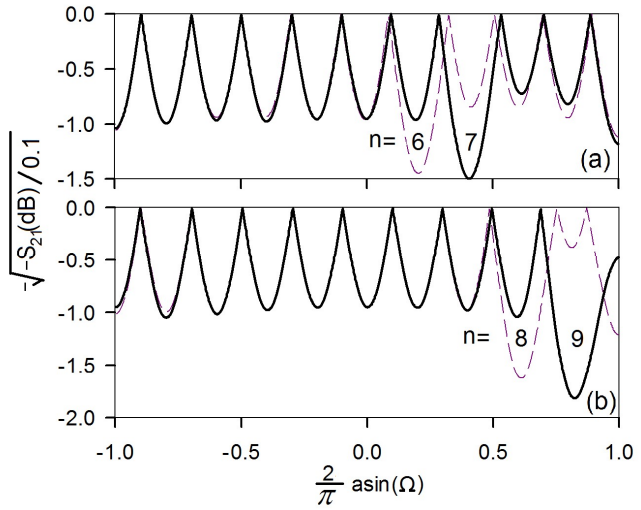

Fig. 3. Result of one iteration on an already optimum filter with all ripple R_n=0.1 dB, resetting the target for one of the ripples R_{0n}, n= 6 ...9 to $\sqrt{R_{0n}} = 1.5\sqrt{0.1}$. The cases n=4 ...1 are determined from the symmetry.

The equations can be tested with the already optimum 10th order filter by resetting one the target ripples, for example R_0 for n=5, leaving the other target ripples as 0.1 dB. This should result in the fifth ripple taking the new value, preferably with the other ripples unchanged. As shown in Fig. 2 and 3, this is approximately correct. Similar curves were produced for filter orders 5, 6, 10, 15 and 20 for ripple levels 0.01, 0.1, and 1 dB. While adjusting one ripple, the other ripples are slightly changed in the opposite direction, so that the main effect is to equalise the ripples instead of setting them to the target value. In particular, when ripple 8 is adjusted, ripple 9 is also changed significantly, but can be corrected in the next iteration. Similarly, when adjusting ripple 7, both 8 and 9 are affected. The other error is that while adjusting ripples 8 or 9, there is a significant overshoot. This is characteristic of the higher order filters, and may be the basis of a future upgrade of the procedure.

In an extreme case where $\sqrt{R_0} \ll \sqrt{R_n}$ and if only one ripple is affected, the level of adjustment ($r_{m,m+1}$-1) or Δf_m varies as $\sqrt{R_n}\,\frac{\alpha}{2N}$ so higher order filters require smaller adjustments. Conversely, the ripple caused by a given error rises as N^2, which makes the starting ripple for higher order filters very large.

Fourier analysis can be introduced, subject to the very approximate nature of the equations. For example, Parseval's theorem (or Rayleigh's theorem) [18] in this context is (taking F_1=-1, F_2=1 and α=1)

$$\sum_{m=1}^{N-1}(r_{m,m+1}-1)^2+\sum_{m=1}^{N}\Delta f_m{}^2 \approx \frac{1}{4N}\sum_{n=1}^{N-1}(\sqrt{R_0}-\sqrt{R_n})^2 \qquad (9)$$

Strictly speaking, there should be a term in (r_e-1) included with the $(r_{m,m+1}-1)$ terms. The equation shows that for a given r.m.s. level of errors, r.m.s. ripple still increases with N, but not as rapidly as in the extreme case above.

To correct the mean ripple level, a further adjustment is performed. Since the filter parameters are, as found numerically, related to the square roots of the ripples, a mean level is given as

$$R_{av}=\left(\frac{1}{N}\sum_{n=1}^{N-1}\sqrt{R_n}\right)^2 \qquad (10)$$

The variation of normalised coupling coefficient for a 10th order Chebyshev filter is given in Fig. 4, based on data from [17]. Since ~~R_n~~R_0 is in dB and the scale is logarithmic, the horizontal variable varies as lg(-20lg|$S_{21}(f_n)$|), where is f_n is at a ripple dip. Between 0.01 and 1 dB,

$$k_e \approx 0.46(1-0.83\lg(R_0)) \qquad (11)$$

So, to change the ripple level from R_{av} to R_0, k_e should be multiplied by a factor

$$p_{e0}=\frac{1-0.83\lg(R_0)}{1-0.83\lg(R_{av})} \qquad (12)$$

but since R_{av} is only an average value, this is only approximate and likelihood of overshoot is reduced by using a partial compensation

$$p_e=\frac{1-0.83\lg(R_0)}{1-0.83\,[\beta\lg(R_{av})+(1-\beta)\lg(R_0)]} \qquad (13)$$

where β is typically α or less. Similarly k_{12} and k_{23} are corrected by factors

$$p_{12} = \frac{1-0.21\,\lg(R_0)}{1-0.21\,[\beta\,\lg(R_{av})+(1-\beta)\lg(R_0)]} \qquad (14)$$

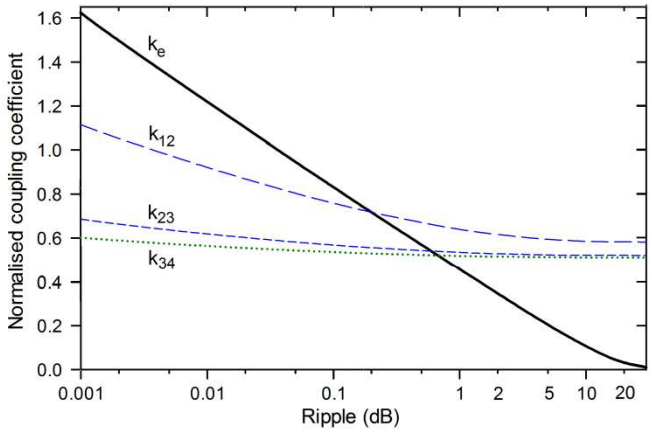

Fig. 4. Variation of normalised coupling coefficient (B/f_0=1) for a 10th order filter. (The x axis is a log scale in addition to dB units being already logarithmic).

$$p_{23} = \frac{1-0.08\,\lg(R_0)}{1-0.08\,[\beta\,\lg(R_{av})+(1-\beta)\lg(R_0)]} \qquad (15)$$

which differ only by the coefficients 0.21 and 0.08. For p_{34} and p_{45}, they are small, 0.04 and 0.03 respectively, so p_{34}, p_{45} … are ignored, that is taken as 1.0. Thus in any single iteration, the initial values of resonant frequencies are shifted by Δf_m (m=1…N) while k_e, k_{12}, …. are replaced by $k_e r_e p_e$, $k_{12} r_{12} p_{12}$, $k_{23} r_{23} p_{23}$, $k_{34} r_{34}$, $k_{45} r_{45}$ … using (1-8) and (13-15). These correction factors hold approximately for filters of other orders, and very crudely for ripple exceeding 1 dB.

The square root and logarithmic dB units in (1) are not completely arbitrary. The response of a filter is

$$|S_{21}|^2 = \frac{1}{1+\varepsilon^2\, C^2(f)} \qquad (16)$$

where $C(f)$ is the Chebyshev (or some other) polynomial. Using $\ln(1+x) \approx x$, $2.3\lg(1+x) \approx x$ for small x, and taking f at the centres of the ripple dips,

$$\sqrt{R_n} \approx 2.08\,|\varepsilon C(f_n)| \qquad (17)$$

Meanwhile, using $|S_{11}|^2 + |S_{21}|^2 = 1$,

$$\left|\frac{S_{11}}{S_{21}}\right|_n = |\varepsilon C(f_n)| \approx \frac{\sqrt{R_n}}{2.08} \qquad (18)$$

Thus (1) could have been written

~~$A_n = \left(\left|\frac{S_{11}}{S_{21}}\right|_0 - \left|\frac{S_{11}}{S_{21}}\right|_n\right)\frac{\alpha}{N}$~~ $A_n =$

$$\left(\left|\frac{S_{11}}{S_{21}}\right|_0 - \left|\frac{S_{11}}{S_{21}}\right|_n\right)\frac{\alpha}{N} \qquad (19)$$

with a small change in α, but $\sqrt{R_n}$ is retained because responses in dB are readily available in commercial e.m. simulators. However, $\left|\frac{S_{11}}{S_{21}}\right|$ has the advantage of being less obscured when there are large resistive losses.

3. Numerical examples

To observe the convergence of the iterative procedure, hypothetical examples were computed using the coupling matrix [1]. As a starting point, Chebyshev filters of various orders had their coefficients varied by arbitrary amounts, so that the ripple increased to either 18 dB or 5 dB, within the constraint that k_e and k_{12} should be reduced so that all the ripples were visible. Repeated iterations then brought the ripple down to 0.01±20% dB or 0.1±20% dB respectively. The dashed line in Fig. 2(a) shows a response with ripple 5 absent. This could be represented as a negative value for $\sqrt{R_5}$, but Fig. 2 was not available at first so such ripples were recorded as zero. The results are given in table 2. Up to 16th order, convergence rates are 1.9 or better. They are somewhat dependent on operator skill in choosing α and β.

Table 2: Chebyshev filter: convergence of the iterative adjustments

(a) Convergence factor: geometric mean value of [Initial Ripple error (dB)/Final Ripple error (dB)] for 1 iteration

	No. of iterations		Convergence Factor (a)	
Max. Start Ripple (dB)	**18**	**5**	**18**	**5**
End Ripple (dB)	**0.01 ±0.002**	**0.1 ±0.02**	**0.01 ±0.002**	**0.1 ±0.02**
Filter order				
3	3	2	21	16
4	6	3	4.6	6.3
5	8	3	3.1	6.3
6	7	3	3.7	6.3
7	8	4	3.1	4.0
10	8	4	3.1	4.0
15	14	8	1.9	2.0
16	14	8	1.9	2.0
20	24	10	1.5	1.7

~~Overall, computation is faster for lower filter orders for several reasons.~~

~~1. The initial ripple error is much smaller, with the lower sensitivity to errors in parameters.~~

~~2.1. With a few exceptions, the table shows a trend for faster convergence.~~

~~3.1. Computation times of e.m. simulators decrease with the lower circuit complexity, perhaps by the square or the cube of the number of resonators.~~

~~Results for cascaded quadruplets (CQs) are given in table 3. In some cases the frequency corrections involving F_1 and F_2 in (4) and (6) had not yet been~~

Table 3: Cascaded quadruplets

Maximum starting ripple: 18 dB,
except for e.m. simulation, 17 dB.

(a) Two quadruplets and 2 other resonators; unknown additional cross coupling. Full e.m. simulation.

(b) All filters are symmetrical, so only cross-couplings on the left-hand side have to be specified.

(c) Typical coupling coefficient in the main path is 0.5 – 0.7.

(d) The ratio of transition region width of the cascaded quadruplet filter to the transition region width of a Chebyshev filter with the same order; measured at @ the attenuation level given in dB.

(e) Convergence factor: geometric average value of [Initial Ripple error (dB)/Final Ripple error (dB)] for 1 iteration

Order	Cross-Coup Coeffts (b),(c)	Skirt Width Ratio (d)	End Ripple (dB)	No. of itera-tions	Conver-gence Factor (e)
4	k14 = -0.126	0.55@39		6	4.6
8	k14 = -0.100	0.65 @60 0.50@83	**0.01 ±0.002**	14	1.9
4	k14 = -0.242	0.49@27		8	3.1
8	k14 = -0.200	0.38@52	**0.01 ±0.002**	19	1.6
12	k14 = -0.187, k58 = -0.155	0.45@60 0.37@76		21	1.5
8	k14 = -0.357	0.24@35		16	1.5
16	k14 =- 0.250, k58 = -0.200	0.34@60 0.24@104	**0.1 ±0.02**	28	1.3
10 (a) e.m. sim			0.015 – 0.064	11	1.7

Table 4: Folded cross-coupled
Maximum starting ripple: 18 dB.
See notes in table 3.

Order	Cross-Coup Coeffts (c)	Skirt Width Ratio (d)	End Ripple (dB)	No. of itera-tions	Conver-gence Factor (e)
6	k25 = -0.106	0.51@46	0.01 ±0.002	11	2.3
6	k25 = -0.2, k16 = 0.03	0.39@47	0.01 ±0.002	13	2.0
6	k25 = -0.33, k16 = 0.085	0.32@34	0.01 ±0.002	16	1.8
12	k58 = -0. 2795 k49 = 0.0443 k3,10 = -0.00244	0.56@60 0.38@101	0.003 to +0.022	24	1.4

Table 5: Cascaded triplets
Maximum starting ripple: 18 dB,
*Conjoined triplets

Or-der	Cross-Coup Coeffts (c)	Skirt Width Ratio (d) Left, Right @ atten (dB)	End Ripple (dB)	No. of itera-tions	Conver-gence Factor (e)
6	k13=-0.25	1.52, 0.50 @ 60 1.71, 0.36 @ 85	0.01 ±0.002	11	2.3
7*	k13=-0.45 k35=-0.35	2.51, 0.14 @ 53	0.1±0.02	23	1.3
9	k13=-0.4 k46=-0.15	1.38, 0.29 @ 60 1.69, 0.22 @ 92	0 to 0.18	8	1.8

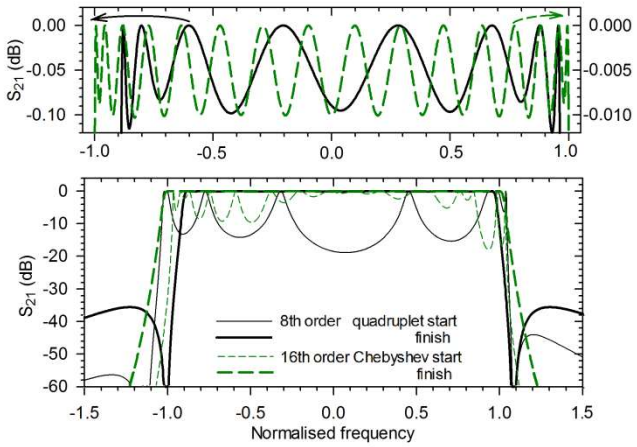

Fig. 5. Initial and final ripple of an 8th order cascaded quadruplet filter and a 16th order Chebyshev filter. Top graph shows the final pass band, expanded.

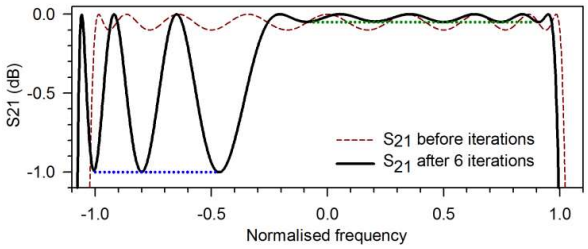

Fig. 6. Starting and final ripple of a 9th order filter with uneven ripple.

Overall, computation is faster for lower filter orders for several reasons.

1. The initial ripple error is much smaller, with the lower sensitivity to errors in parameters.
2. With a few exceptions, the table shows a trend for faster convergence.
3. Computation times of e.m. simulators decrease with the lower circuit complexity, perhaps by the square or the cube of the number of resonators.

Results for cascaded quadruplets (CQs) are given in table 3. In some cases the frequency corrections involving F_1 and F_2 in (4) and (6) had not yet been incorporated, and making an overall scaling at the end of the iterative process, the final values of the cross-coupling coefficients are not the initial values. Convergence is workable with moderate cross coupling coefficients sufficient to reduce significantly the transition region compared Chebyshev filters of the same order. For higher orders and strong cross coupling, the ripple either did not converge or converged very slowly at 0.01 dB, so a less ambitious target of 0.1 dB is recorded.

Finally, results for the folded, cross-coupled configuration and for cascaded triplets (including one filter with conjoined triplets) are given in tables 4 and 5, with similar conclusions.

The initial and final responses of two of the filters, a 16th order Chebyshev and an 8th order CQ filter, are given in fig. 5. Both have reached their target ripple. The frequency and bandwidth corrections in (4) and (6) were incorporated in the case of the Chebyshev filter, and the accurate final

bandwidth ~~of the former case~~ is evident, in contrast to the ~~latter~~CQ filter. The CQ coefficients are recorded in table 6. The resonant frequencies are within 0.00007 normalised units of each other. For the 16th order filter, the coefficients are within 0.001 dimensionless unit of the theoretical values, despite a remaining ±20% error in the ripple level. This illustrates the error sensitivity of higher order filters.

A filter with non-uniform ripple (three 1 dB and six 0.05 dB ripples) is shown in fig. 6, showing the adaptability of the procedure. The coefficients are given in table 6. A more realistic situation is where ripples near the band edges either need to be smaller to reduce error sensitivity [19], or have a relaxed requirement when the signal spectral content is smaller at the band edges. In another application, a measured filter may have a certain ripple pattern. Setting the target ripple to these values, the algorithm can be used ~~together with coupling matrices~~ to find the actual filter coupling coefficients and resonant frequencies, for comparison with the intended values.

Table 6: Coupling coefficients of an 8th order CQ filter, and a 9th order filter with non-uniform ripple

	CQ	Non-uniform ripple		CQ	Non-uniform ripple
f_1	0.03755	0.1147	k_e	0.7726	0.7614
f_2	0.03750	-0.0189	k_{12}	0.6163	0.7100
f_3	0.03747	-0.0480	k_{23}	0.7414	0.5866
f_4	0.03748	-0.0165	k_{34}	0.3907	0.5338
f_5	NA	-0.0625	k_{45}	0.4784	0.5380
			k_{14}	-0.33	NA

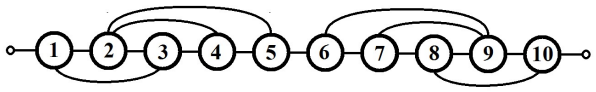

(a)

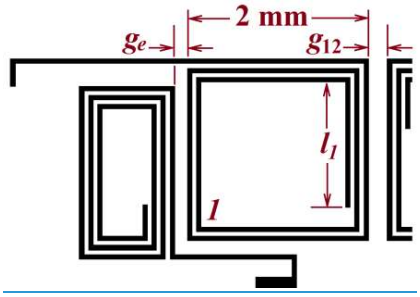

(b)

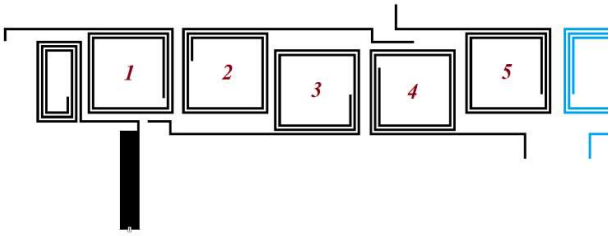

(c)

Fig. 7 (a). *Architecture of the superconducting spiral filter, showing all the intended coupling. (b) Enlargement of one spiral, showing definition of the lengths and gaps. (c) Layout of the left-hand half of the (symmetrical) filter.*

4. Full filter design example: superconducting spiral filter

A spiral microstrip superconducting filter was designed for the radio telescope in Yebes, Spain, with 2295 MHz centre frequency and 7% bandwidth; further details will be given with the results. The substrate is 0.5 mm thick Magnesium Oxide, coated on both sides with 600 nm of Yttrium Barium Copper Oxide (YBCO) and further coated with 200 nm of Gold, from which the small terminals for contact with the external circuit are fabricated; the gold was removed everywhere else as it is lossy. The eventual circuit has dimensions 30 mm x 8 mm including some empty space between the spirals and the box walls. Other details are similar to [20].

The specified frequency response is asymmetrical, but satisfied by an 8th order CQ symmetrical response; 10th order was chosen for a larger error margin. The extra substrate area including the increased empty space is small, about 5 x 8 mm^2, similar to the hexagonal footprint of an SMA connector. ~~The design procedure is well established [21], [1] based on the coupling matrix, with the~~target coupling coefficients including cross coupling were found ~~in this case~~ by trial and error, starting with Chebyshev coupling coefficients and evaluating S_{21} and S_{11} with the coupling matrix [21], [1], because the foregoing ~~design~~iterative procedure was not yet completed. The architecture showing all the intentional coupling coefficients is given in Fig. 7(a). The chosen resonators are 2½ turn spirals with dimensions 2 x 2 mm^2, with track width 0.05 mm (Fig. 7(b,c)). Resonant frequencies and coupling coefficients found from full wave SONNET [22] simulations were used for the initial design. Simulations of the whole filter showed a significant asymmetry in the frequency response, as anticipated, due to cross coupling between non-adjacent resonators. Winding direction (moving inwards towards the centre of the spiral) is clockwise for resonator 1, anticlockwise for resonators 2 and 3, and clockwise for resonators 4 and 5, with the remainder of the layout symmetrical. This causes the magnetic and electric coupling between resonators m and m+2 to have opposite signs [23], so that the unwanted cross coupling could be at least partially cancelled by introducing additional cross coupling k_{13} and k_{24} as shown in Fig. 7(a). The cross-coupling k_{25} for the CQ section is also negative, as required. Since the design procedure does not provide calculations for cross coupling, they are not optimised, but only determined by trial and error to produce suitably low side-lobes, with an error margin to allow variations as the pass band was iteratively adjusted, but in this case, the side-lobe level was further decreased. Since the specification itself is asymmetrical, a simpler strategy may have been to make full use of the naturally occurring coupling $k_{m,m+2}$ and ~~omit the~~not have CQ sections. However, the architecture used does suggest that a range of architectures are available for other filter specifications.

~~Finally, the~~After the sidelobes were set, k_e and k_{12} were decreased to ensure that all 9 ripples were visible. The design procedure was invoked to reduce the ripple from 17 dB to the 0.05 dB target, again giving an error margin.

Equations (4), (5), (6), (13), (14) and (15) give the estimated correction for resonator centre frequency and coupling coefficient. The changes in resonator dimensions (Fig. 7(b)) are then

$$\Delta l_m = \frac{80}{-120}\Delta f_m \quad \text{mm} \qquad (20)$$

where the filter half-bandwidth is 80 MHz and the rate of change of resonant frequency is -120 MHz/mm, as found from simulations. The gap and coupling coefficient are related approximately logarithmically so an interpolation equation for gaps g_e, g_{12}, g_{23}, g_{34}, g_{45} and g_{56} mm is

$$\frac{\Delta g}{0.1} = \frac{\log(r)}{\log(r')} \qquad (21)$$

where r is one of the values $r_e p_e$, $r_{12}p_{12}$, $r_{23}p_{23}$, r_{34}, r_{45} and r_{56}, as given earlier, and r' is the corresponding value for a 0.1 mm increase in the gap, given in table 7. Except for r_e' and r_{34}', each gap remained in one of the ranges given in the table. The number of iterations and the final resonator dimensions and spacings are given in tables 8 and 9. The huge initial ripple is no great drawback: the additional iterations are done with the coarse, fast setting. The cell size was progressively decreased not only for improved accuracy but also finer control over gaps and resonator lengths without resorting to the fine tuning described in [24]. The approximate assumption that each dimension (gap or length in fig. 7(b) affects only one parameter (coupling coefficient or resonance frequency) may slow the convergence in lower order filters where the expectation for convergence is higher. Furthermore, a large adjustment in F_1 or F_2 may introduce further ripple which has to be adjusted in the next iteration.

The superconducting filter used an earlier, more cumbersome version of the algorithm, but when re-designed using the foregoing equations, the dimensions were within 0.0025mm, the final simulation cell size, so it is a valid demonstration. Performance at 20 Kelvin is compared with

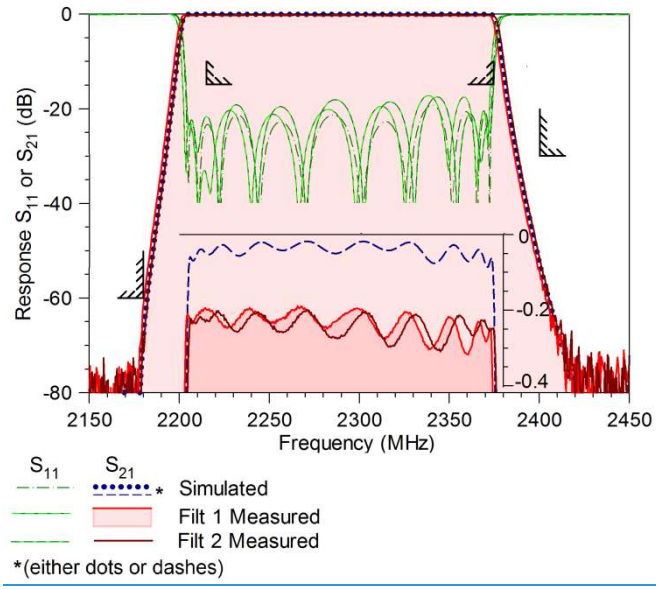

(a)

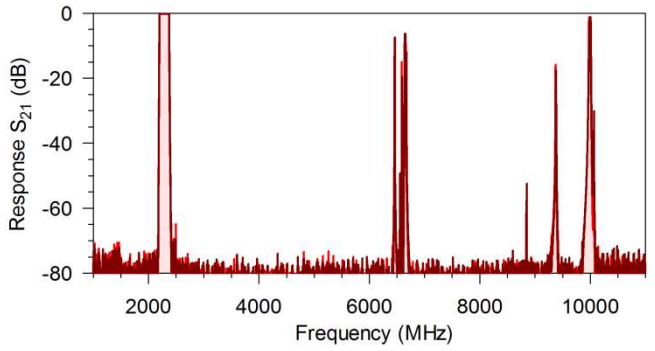

(b)

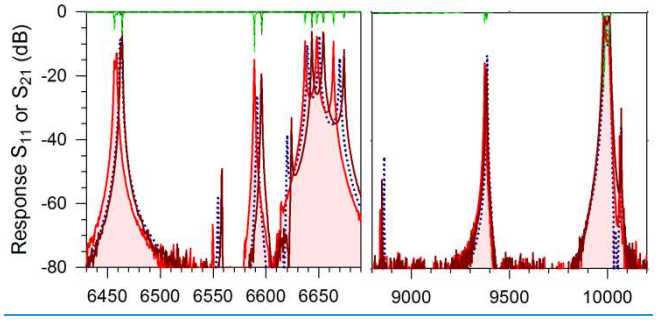

(c)

Fig. 8 (a). *Simulated and measured pass band characteristics of the filter, together with the specification. (b) Stop band response (c) enlargement of the spurious responses. All share the same legend.*

simulations and specifications in Fig. 8. The main error is a frequency shift. Previous experience suggested a small discrepancy between simulations and measurements; also attempting to allow for different simulation cell size, temperature and frequency band, the filter was designed anticipating that the measured response would be 7 MHz higher than the simulations. However, the discrepancy is much less. The error margin is 5 MHz, so there is a 2 MHz encroachment on the upper passband edge by one of the filters, and 0.3 MHz by the other, out of the 160 MHz pass band. The stop band limit at 2180 MHz is not violated. ~~A 7 MHz adjustment requires the lengths l_n to be shortened by 0.06 mm, together with one further iterative adjustment. With the filters already fabricated, a 2 MHz adjustment can be produced by placing the lid 2 mm above the substrate, or perhaps by tuning screws.~~A 7

~~In all other respects, the filter matches specifications well. The ripple is about 0.1 dB, compared with the 0.05 dB target and the 0.14 dB specification. The asymmetry in the transition regions is commensurate with the specification, and the side lobes are lower than the measurement noise floor.~~

Table 7. The variation of coupling coefficient (expressed as a ratio) for a 0.1mm increase in gap

Gap (mm) range g_a to g_b	External coupling r'_e	Internal coupling, tails inwards	Internal coup. tails outwards
0.1 to 0.2	~~r'_e:~~ 0.621	~~r'_{34}:~~	r'_{23}: 0.685
0.2 to 0.3	~~---~~ 0.671	0.769	r'_{45}: 0.719
0.3 to 0.4	~~---~~ 0.709	r'_{12}, r'_{34}, r'_{56}: 0.775	-- 0.735
0.4 to 0.5	0.735	--- 0.781	

$$r_e' = \frac{k_e(g_e=g_b)}{k_e(g_e=g_a)}; \quad r_{12}' = \frac{k_{12}(g_{12}=g_b)}{k_{12}(g_{12}=g_a)}; \ \ldots$$

Table 8: No. of iterations for spiral filter simulated by SONNET:

Total CPU time: 8 ½ hrs

Segmentation	Cell size (μm)	No. of iterations	Time per iteration	Approx. final ripple (dB)
Edge mesh	10	6	5 min	0.3
Edge mesh	5	3	18 min	0.1
Fine mesh	2.5	2	3.5 hours	0.06

Table 9. Final dimensions of the filter

Resonator No, n	l_n (mm)	Length of tail (mm)	Gap no.	Gap (mm)
1	1.3825	2.20	External	0.1400
2	0.5175	3.70	12	0.2100
3	0.6975	2.25	23	0.1450
4	1.320	2.20	34	0.2275
5	1.290	2.20	45	0.2350
			56	0.2925

MHz adjustment requires the lengths l_n to be shortened by 0.06 mm. With the filters already fabricated, a 2 MHz adjustment can be produced by placing the lid 2 mm above the substrate, or perhaps by tuning screws.

In all other respects, the filter matches specifications well. The ripple is about 0.1 dB, compared with the 0.05 dB target and the 0.14 dB specification. The asymmetry in the transition regions is commensurate with the specification, and the side lobes are lower than the measurement noise floor.

Resonator resistive losses result in a gentle variation of |S21| in addition to the ripple, so that the ripple peaks at the band edges are about 0.025 dB lower than at the centre. By matching this in the simulation, the estimated superconductor surface resistance is 10 μΩ per square (assuming negligible dielectric loss) and the quality factor of the resonators is approximately 70,000, consistent with previous work [21], [23]. The remainder of the loss, about 0.2 dB, is believed to be in the external conductors, including ~~non-metallic~~ epoxy conducting glue and a male-to-male adaptor, and to calibration: a re-measurement (using equipment at the laboratory of one of the other authors) yielded a value of 0.1 dB.

The wideband response is shown in fig. 8(b), vindicating the choice of spirals for the wide stop band. The close-up of the higher order responses is given in fig. 8(c), confirming that the simulator is working well, and opening the possibility of suppressing these responses. The filter packaging appears in fig. 9. The silvery conducting glue increases the width of the input line, which may have contributed to the somewhat large passband S_{11}.

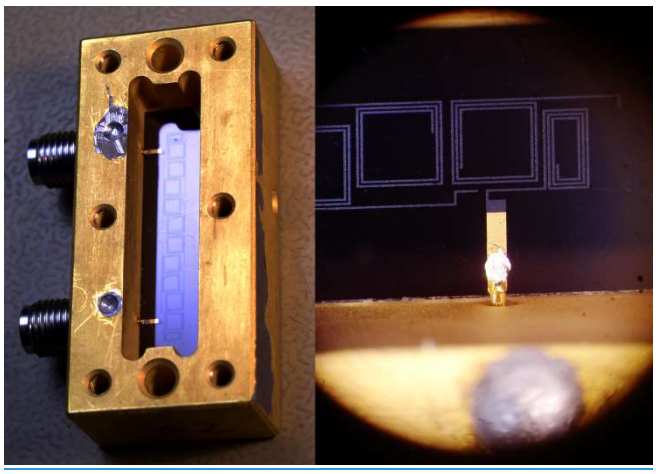

(a) (b)

Fig. 9(a) *The filter, fully assembled except for the cover, and (b) a close-up of the right-hand side. Contrast has been artificially enhanced to show the black spirals above the black ground plane. Nevertheless, in (a), it is the shadows of the spirals that are visible, rather than the spirals themselves.*

In the simplest version of the existing optimisation algorithm, the Jacobian matrix is computed using full wave simulations. The 10th order filter has 11 parameters, k_e, $k_{m,m+1}$ and Δf_m (m=1 … 5), to be adjusted to determine 9 ripples together with filter centre frequency and bandwidth. However, the relationship between mean Δf_m and centre frequency, and between mean coupling coefficient and band width, is obvious, leaving effectively 9 parameters to be related to 9 ripples. This requires 10 simulations, one with the starting parameters and then a further nine each with one parameter changed. The matrix may vary as the ripple decreases so it may have to be re-evaluated towards the end of the iterative process, to minimise the number of time consuming iterations using the fine mesh. The Jacobian matrix itself would probably be computed using coarse or medium accuracy, as only the gradients are required. Even if only 4 iterations are used, it requires an initial simulation, plus one more after each iteration, giving a grand total of 25 simulations.

The present method~~, which is at its best for small ripple (admittedly not down to 0.01 dB) to reduce the number of high-accuracy simulations, finished in~~ used 11 iterations. Adjusting the cross coupling and the initial setting of k_e and k_{12} to make the ripples visible has been omitted in the comparison.

5. Speculative Explanation

The ripple optimisation is based on numerical fitting, but a speculative explanation may be the basis of a future theory. A microstrip filter of straight half-wave transmission line resonators separated by capacitive gaps is shown in Fig. 10(a). The signal shown, initially propagating to the right, is reflected at each gap with only a small part of the energy transmitted. It traverses resonator 1 several times and the combined transmission at gap 12 forms the propagating wave passing to resonator 2, where it also reverberates before being fully transferred to resonator 3. Thus the filter has greatly enhanced delay (or equivalently, phase slope)

compared with a plain transmission line. In the pass band, correct choice of the gaps ensures that the reflection S_{11} is small. Phase slope of S_{21} increases with N and reciprocal of bandwidth, with lag increasing by $N\pi$ radians [25] as frequency increases across the pass band and transition regions, so not all this phase shift is in the pass band. As a delay line, it has drawbacks of limited bandwidth, dispersion, and non-constant amplitude. Nevertheless it has been used for a delay line ("transversal") filter [25], [26].

If the reflection coefficient at gap 34 at the centre of the filter increases slightly, S_{11} is different by an excess amount ΔS_{11}. ΔS_{11} and S_{21} have equal phase slope, as they traverse equal distances within the filter. Gap 34 is effectively the reference plane for reflections when considering $\Delta S_{11}/S_{21}$ which has zero phase slope; it shifts S_{11}/S_{21} vertically by a constant amount (the dotted to the solid line in Fig. 10(b)), resulting in unequal positive and negative ripples. $|S_{11}/S_{21}|$ (dashed lines) then has alternating large and small ripples, which explains Fig. 1(c). Similarly, if the gaps "*e*" (or gaps 12 and 56) are incorrect (Fig. 10(c)), the two excess reflections with their different phase shifts interfere constructively or destructively, giving $\Delta S_{11}/S_{21}$ with a similar number of cycles to the optimum S_{11}/S_{21}. $|S_{11}/S_{21}|$ has a constant or slowly varying excess ripple, as shown in Fig. 1(a). The explanation for errors in resonant frequency is assumed to be similar. Thus the filter is viewed as a delay line, and two symmetrically situated errors lead to two echoes in the time domain, whose delay difference determines a cosine envelope of the filter ripple in the frequency domain. A closer examination of filter dispersion may yield a more accurate formulation.

6. Conclusion

A procedure for iterative adjustment of filter ripple has been proposed, based on empirical formulae. The emphasis is on simplicity, but refinements are suggested. It has been successfully applied to the design of a 10th order superconducting filter with spiral resonators for a specific application in a radio telescope.

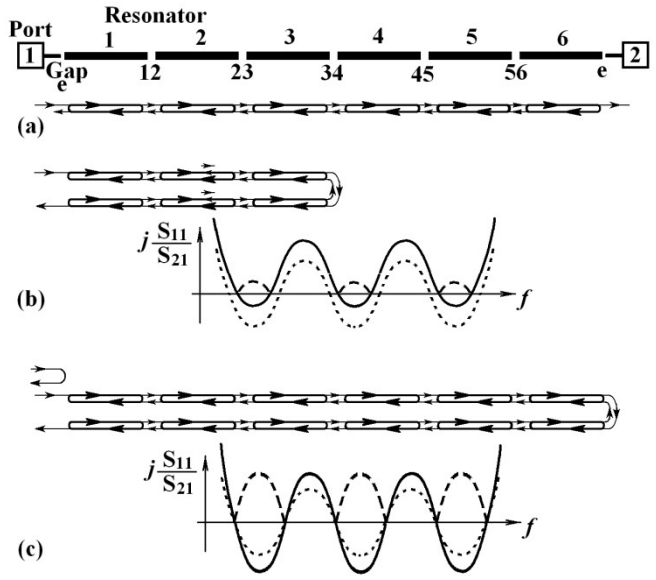

Fig. 10. (a) *End-coupled half-wavelength filter with signal path for S_{21}. (b) Signal path for excess reflection at gap 34, and its effect on S_{11}/S_{21}. (c) Two signal paths, from excess reflection at gaps "e" and their effect on S_{11}/S_{21}.*

7. References

[1] Hong, J.S. and Lancaster, M. J. 'Microstrip Filters for RF/Microwave Applications', Wiley Interscience, 2001.

[2] Cameron, R. J., Kudsia, C. M., and Mansour, R. R., 'Microwave Filters for Communication Systems: Fundamentals, Design, and Applications", Wiley Interscience, 2007.

[3] Bandler, J. W., Chen, S. H., Daijavad, S., and Madsen, K., 'Efficient Optimization With Integrated Gradient Approximations', IEEE Trans. Microwave Theory and Techniques. 1988, 36, (2), pp.444-455.

[4] Garcia-Lamperez, A., Llorente-Romano, S., Salazar-Palma, M., and Sarkar, T. K., 'Efficient Electromagnetic Optimization of Microwave Filters and Multiplexers Using Rational Models' IEEE Trans. Microwave Theory and Techniques. 2004, 52, (2), pp.508-521.

[5] Amari, S., 'Synthesis of Cross-Coupled Resonator Filters Using an Analytical Gradient-Based Optimization Technique', IEEE Trans. Microwave Theory and Techniques. 2000, 48, (9), pp.1559-1564.

[6] Bila, S., Baillargeat, D., Aubourg, M, et al, 'Direct Electromagnetic Optimization of Microwave Filters', IEEE Microwave Magazine, 2001, 2, (1), 46-51.

[7] Swanson, D., and Macchiarella, G., '~~Micrwoave~~Microwave filter design by synthesis and optimization', IEEE Microwave Magazine, 2007, 8, (2), 55-69.

[8] Dishal, M., 'Alignment and Adjustment of Synchronously Tuned Multiple-Resonant-Circuit Filters" Proc. IRE, 1951, 39, (11), pp1448-1455.

[9] Zahirovic, N., and Mansour, R. R., 'Sequential Tuning of Coupled Resonator Filters Using Hilbert Transform Derived Relative Group Delay', 2008, IEEE MTT-S International Microwave Symposium Digest, Atlanta, GA,USA, June 2008, pp 739-742.

[10] Dunsmore, J., 'Tuning band pass filters in the time domain', 1999 IEEE MTT-S International Microwave Symposium Digest, Anaheim, CA, USA, Jun 1999, pp1351-1354.

[11] 'CST – Computer Simulation Technology', https://www.cst.com/, accessed 20 Jul 2017.

[12] 'Filter synthesis software', http://www.nuhertz.com/software/filter-synthesis-software, accessed 10 May 2017

[13] Huang, F., 'Superconducting Spiral Wide Band-pass Filters with Wide Upper Stop-band', IEEE Trans. Microwave Theory and Techniques. 2005, 53, (7), pp. 2335-2339.

[14] Williams, A., 'A Four-Cavity Elliptic Waveguide Filter', IEEE Trans. Microwave Theory and Techniques. 1970, MTT-18, (12), pp. 1109-1114.

[15] Levy, R., 'Direct Synthesis of Cascaded Quadruplet (CQ) Filters', IEEE Trans. Microwave Theory and Techniques. 1995, 43, (12), pp. 2940-2945.

[16] Levy, R., and Petre, Peter, 'Design of CT and CQ Filters Using Approximation and Optimisation', IEEE Trans. Microwave Theory and Techniques. 2001, 49, (12), pp. 2350-2356.

[17] Matthaei, G., Young, L., and Jones, E. M. T., 'Microwave Filters, impedance-matching Networks and Coupling Structures', Artech House Publishers, 1980.

[18] Bracewell, R. N., "The Fourier Transform and its Applications", McGraw-Hill Kogakushu Ltd, 1978.

[19] Jayyousi, R. A. B., Lancaster, M. J., and Huang, F., 'Filtering Functions with Reduced Fabrication Sensitivity,' IEEE Microwave & Wireless Components Letters, 2005, 15, (5), pp. 360-362.

[20] Bolli, P., Cresci, L., Huang, F., Mariotti, S., and Dario Panella, 'A High Temperature Superconductor microwave filter working in C-band for the Sardinia radio telescope', Journal of Astronomical Instrumentation, 2014, 3, (1), pp. 1-16.

[21] Huang, F., 'Ultra-compact Superconducting Narrow-band Filters Using Single and Twin-spiral Resonators", IEEE Trans. Microwave Theory and Techniques. 2003, 51, (2), pp. 487-91.

[22] 'Sonnet', http://www.sonnetsoftware.com/

[23] Huang, F., and Xiong, X., 'Very compact spiral resonator implementation of narrow-band superconducting quasi-elliptic filters', 33rd European Microwave Conference proceedings, Oct 2003 pp. 1059-62.

[24] Swanson D. G., Forse, R., and Nilsson, B.J.L., "A 10 GHz Thin Film Lumped Element High Temperature Superconductor Filter", 1992, IEEE MTT-S digest, Albuquerque, USA, June 1992, pp 1191-1193.

[25] Huang, F., 'A narrowband quasi-transversal filter using a slow-wave structure', 24th European Microwave Conference Proceedings, Sep. 1994, ~~pp478~~pp. 478-83.

[26] Huang, F., 'A novel slow-wave structure for narrowband quasi-transversal filters', IEE Proc. Microwaves, Antennas and Propagation, 1995, 142, (5), pp. 389-93.